Binder-free Nickel Iron Selenide Catalyst arrays for coupling hydrogen production with polyethylene terephthalate plastic electro-upcycling

Pooja J. Sharma[1], Sanjay A. Bhakhar[1], Meghana N. Patel[2], Manish N. Nandpal[2], Kaushik A. Bhakhar[3], Samir G. Patel[2], Parikshit Sahatiya[4], Goli Nagaraju[5], C.K. Sumesh[1], Pratik M. Pataniya[1,*]

[1]*Department of Physical Sciences, P D Patel Institute of Applied Sciences, Charotar University of Science and Technology, CHARUSAT, Changa, Gujarat, India.*

[2]*Department of Pharmaceutical Chemistry and Analysis, Ramanbhai Patel College of Pharmacy, Charotar University of Science and Technology, CHARUSAT Changa, Gujarat, India.*

[3]*Gandhinagar Institute of Pharmacy, Gandhinagar University, Gandhinagar, Gujarat-382721.*

[4]*Department of Electrical and Electronic Engineering, BITS Pilani Hyderabad, Secunderabad-500078, India.*

[5]*Department of Materials, Imperial College London, London, SW72AZ, United Kingdom.*

Email: [*]pm.pataniya9991@gmail.com

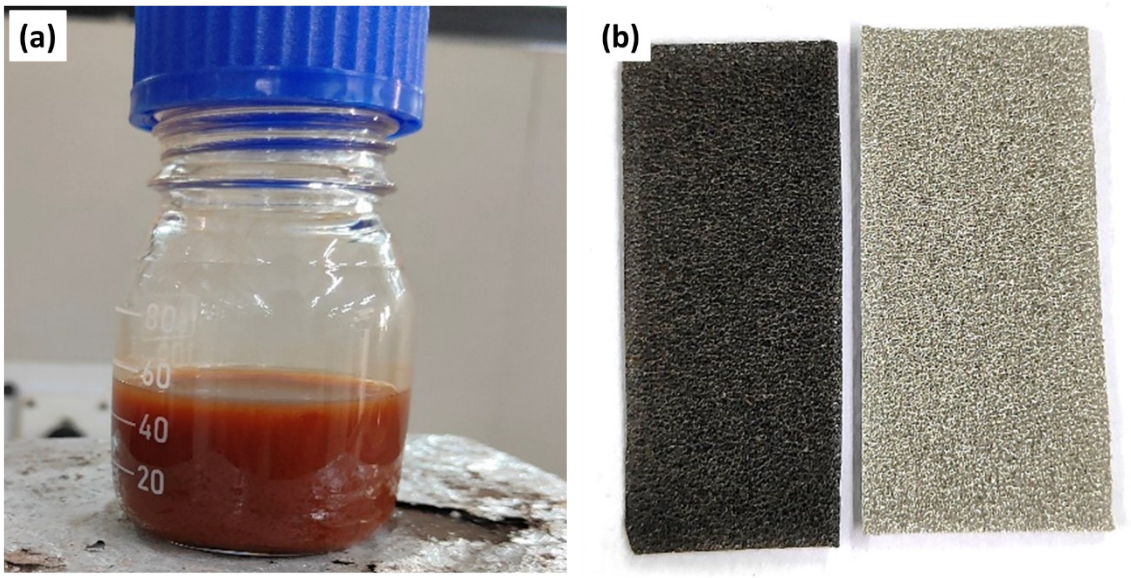

Figure S1 Ni-Fe_3Se_4 precursor solution for chemical bath deposition, (b) Digital image of Ni-Fe_3Se_4 (left) and bare NF (right).

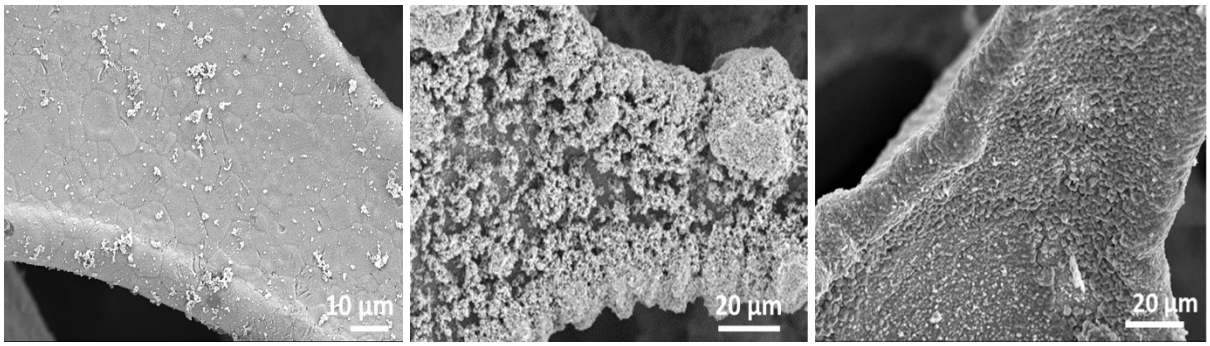

Figure S2 SEM images of NiSe, Ni-Fe_3O_4, Ni-Fe_3Se_4 electrodes, respectively.

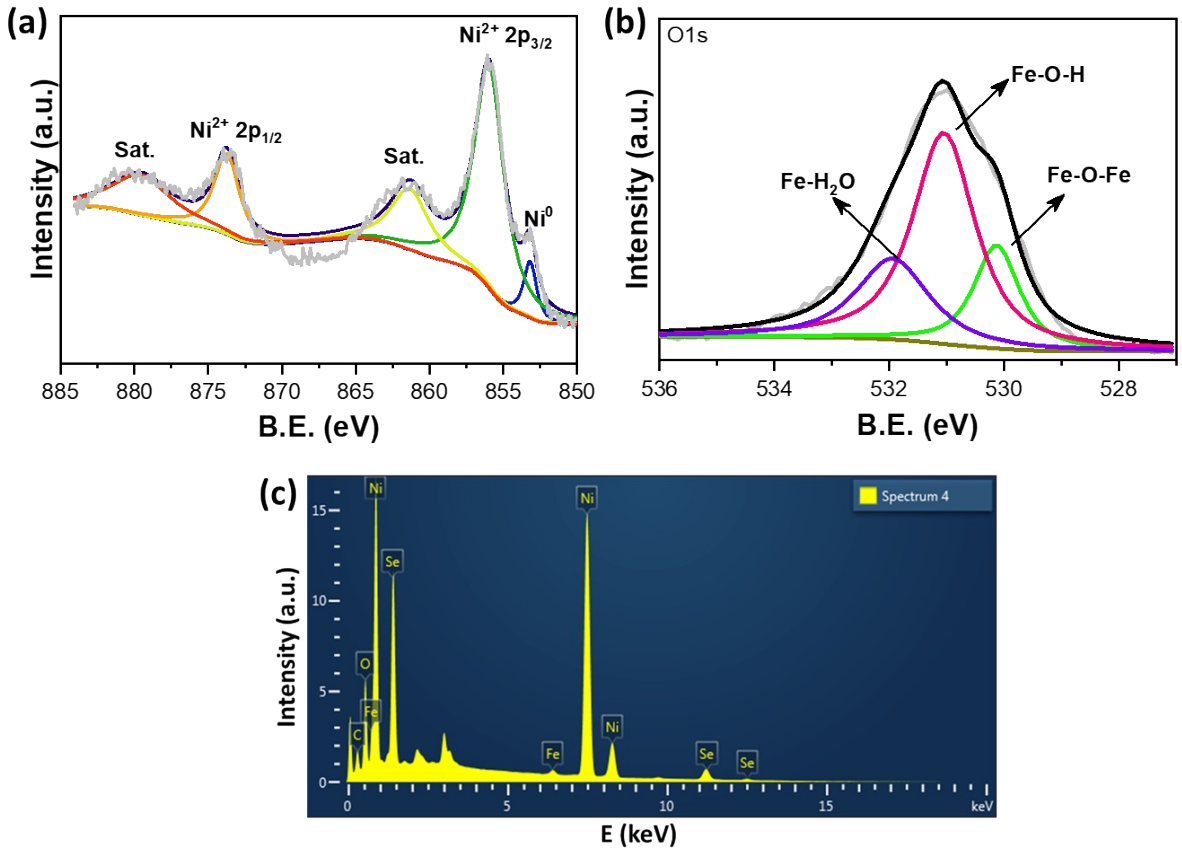

Figure S3 (a) Ni2p, (b) O1s XPS spectra and (c)SEM-EDS pattern of the Ni-Fe_3Se_4 catalyst.

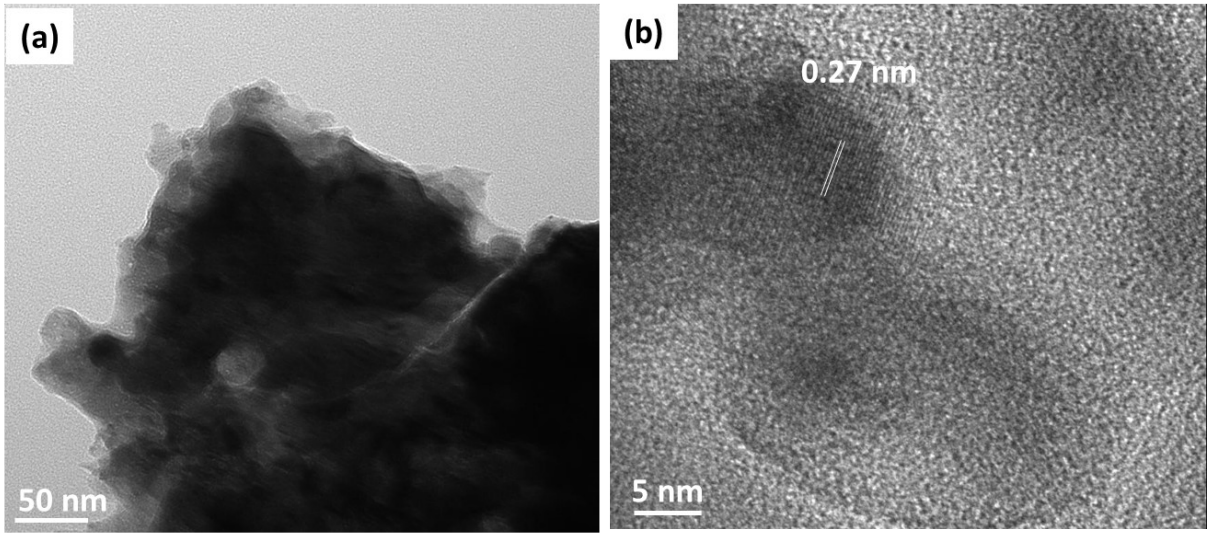

Figure S4 (a) TEM and (b) HRTEM image of Ni-Fe_3Se_4 catalyst.

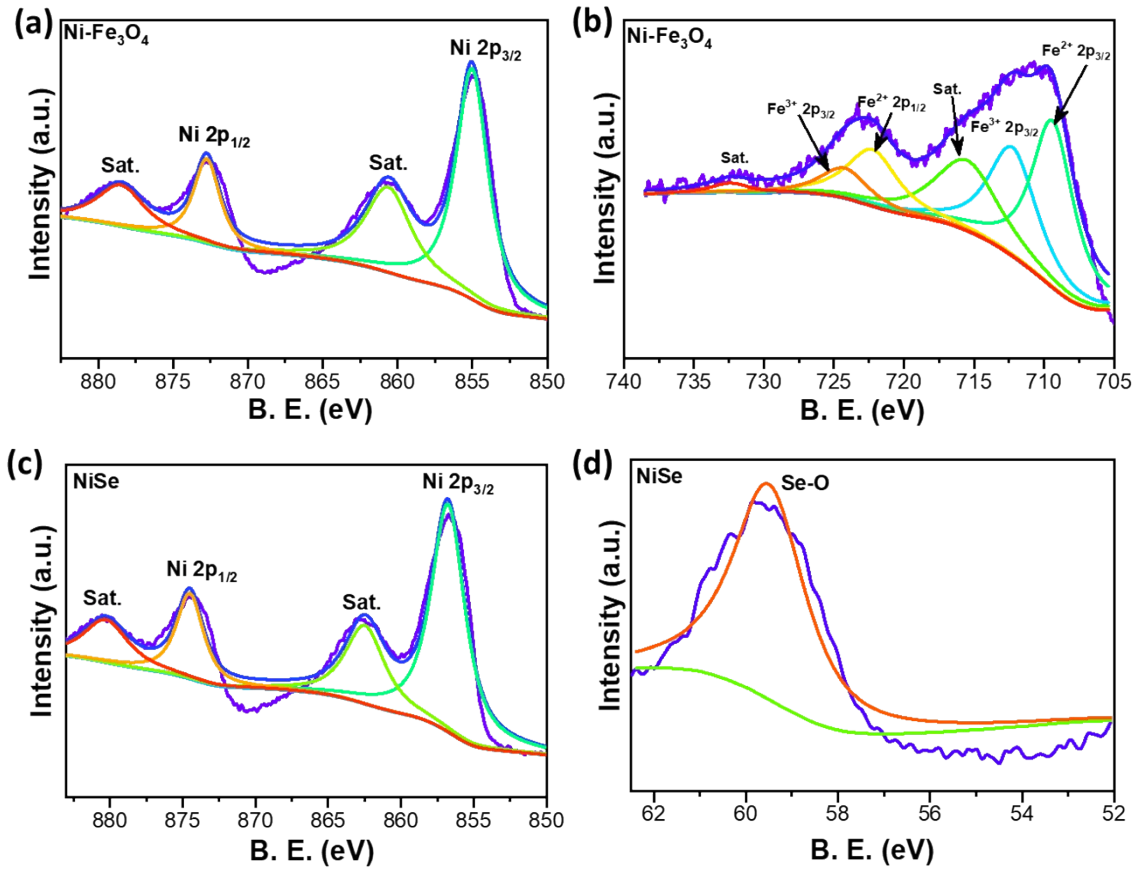

Figure S5 XPS spectra (a) Ni 2p, (b) Fe 2p of Ni-Fe_3O_4 and (c) Ni 2p and (d) Se 3d of NiSe.

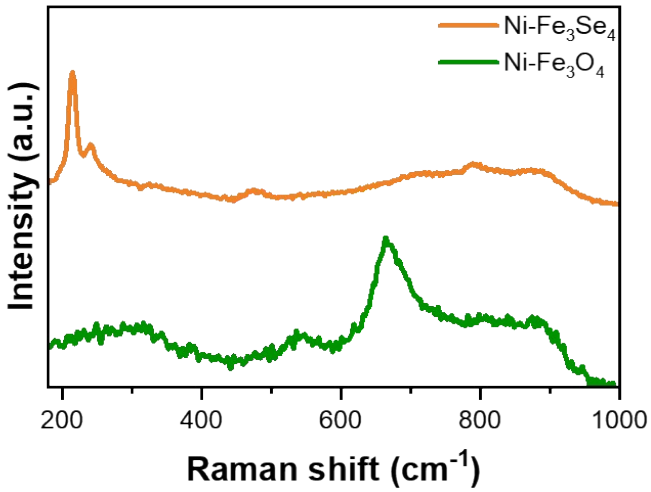

Figure S6 Raman spectra of Ni-Fe_3Se_4 and Ni-Fe_3O_4.

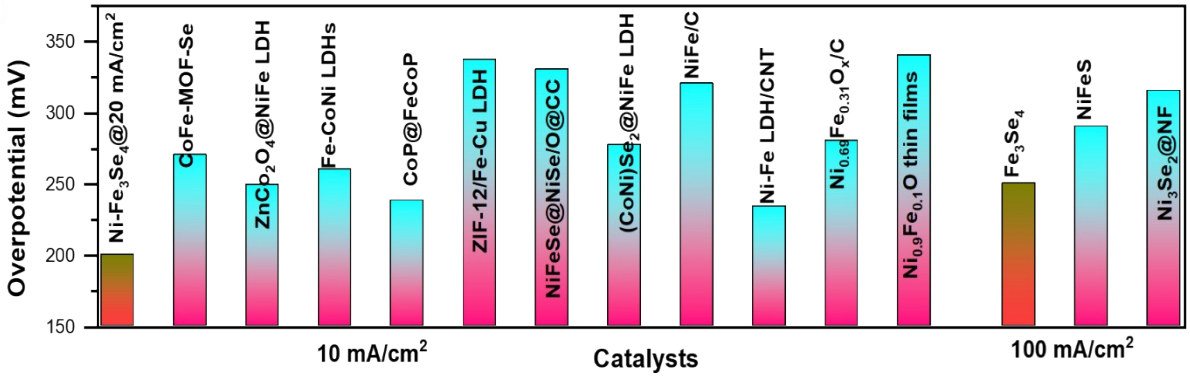

Figure S7 Comparison of OER performance of Ni-Fe_3Se_4 with previous reports[1–13].

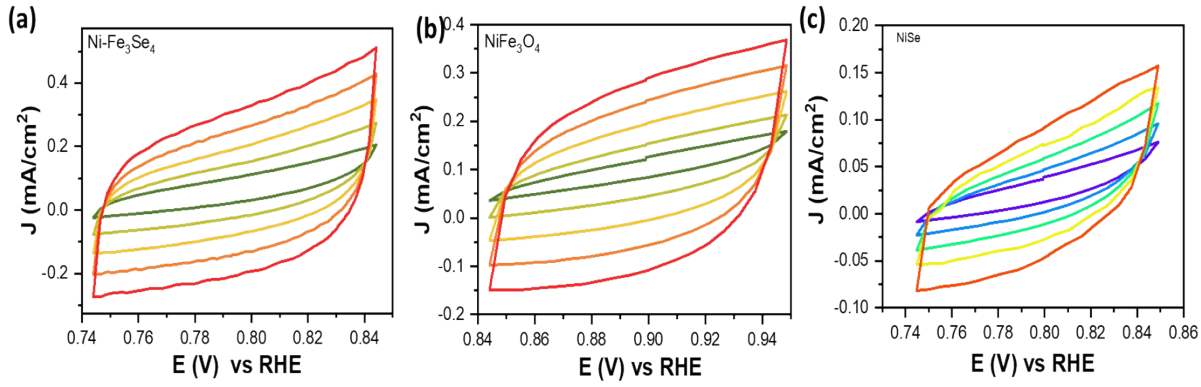

Figure S8 CV-curves recorded in the non-faradic region at different scan rate 20 to 100 mV/s.

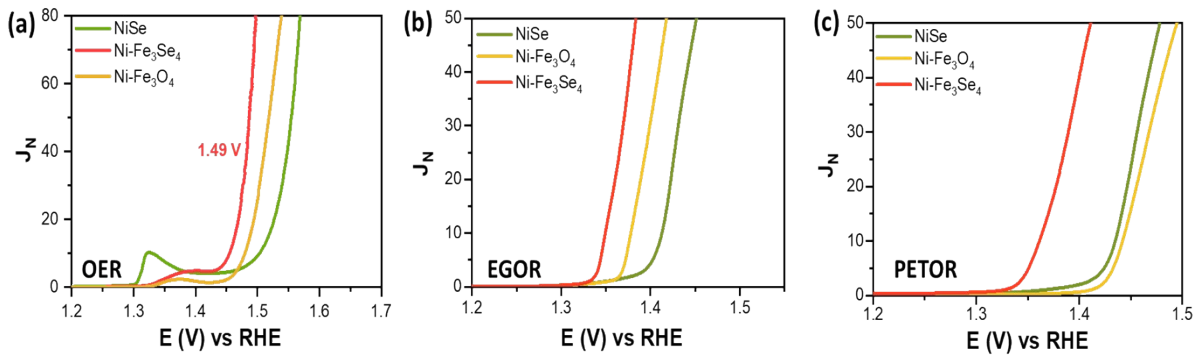

Figure S9 Normalized polarization curves for OER, EGOR and PETOR.

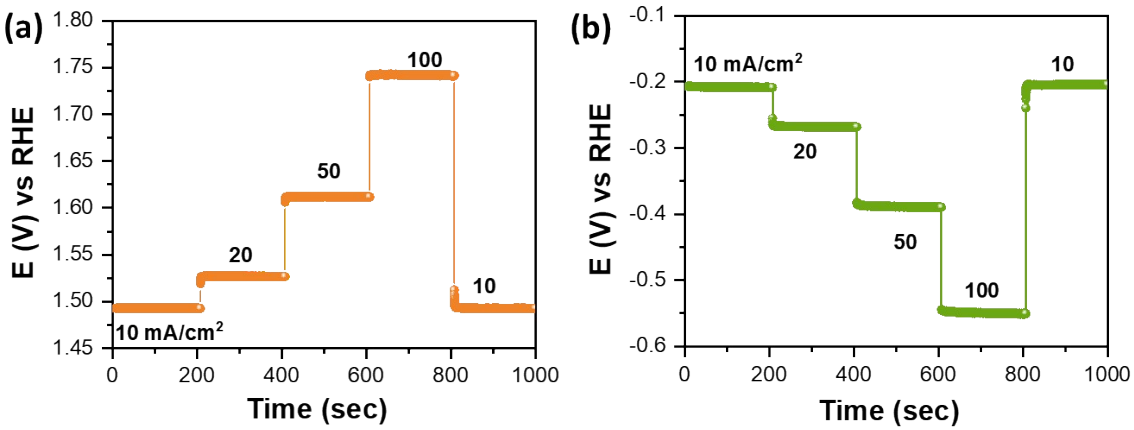

Figure S10 Multistep chrono-potentiometry curve for (a) HER, (b) OER activity on the Ni-Fe_3Se_4 catalyst.

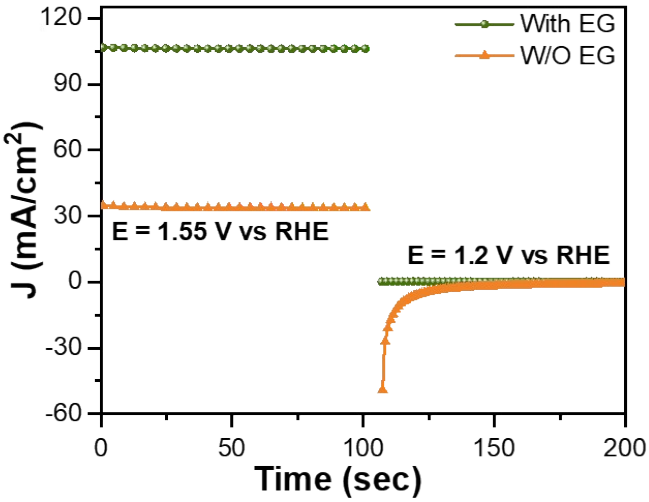

Figure S11 Chrono-amperometry test to study the indirect oxidation mechanism on Ni-Fe_3Se_4.

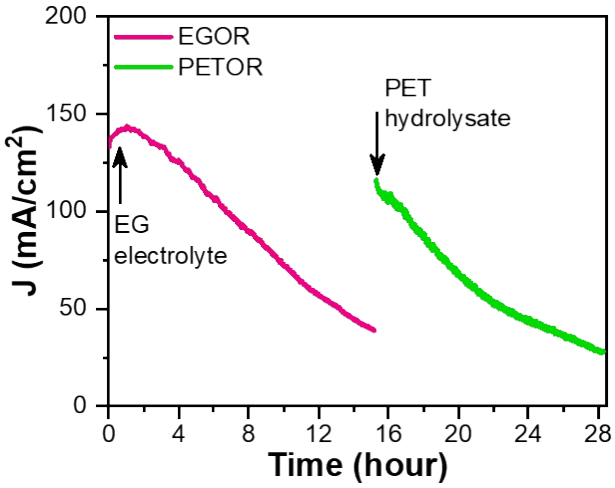

Figure S12 Chrono-amperometry tests for EGOR and PETOR at 1.6 v vs RHE (without iR compensation).

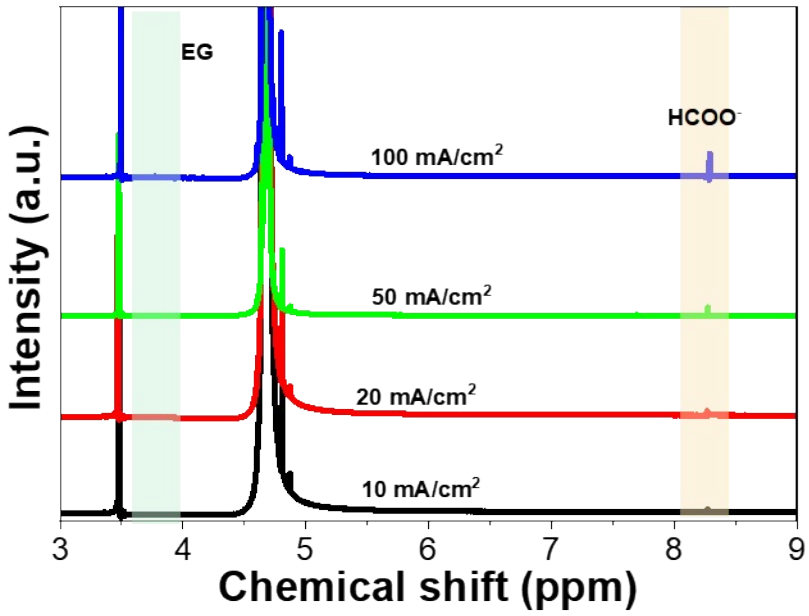

Figure S13 1H NMR spectra of EG after electrolysis at different current densities for 2 hr.

Quantification of Formate and calculation of the faradic efficiency:

For the quantification of the formate in the electrolytes was performed using Shimadzu High-Performance Liquid Chromatographic System, Japan (LC-2010 CHT), equipped with PDA detector fitted with quaternary gradient pump, degasser, column oven and autosampler, Luna C_{18} Column (250 mm×4.6 mm; 5µm). After electrolysis at different current densities (10-100 mA/cm^2), 1 ml electrolyte was diluted in 9 ml HPLC grade water and used for the recording the chromatograph. The calibration curve was also prepared for the quantification of the formate.

Optimized Chromatographic Conditions

Parameters	Experimental conditions
Instrument	Shimadzu High-Performance Liquid Chromatographic System, Japan (LC-2010 CHT), equipped with PDA detector fitted with quaternary gradient pump, degasser, column oven and autosampler
Column	Luna C_{18} Column (250 mm×4.6 mm; 5µm)
Mobile phase	27.5 mM H_2SO_4 (0.75 mL of H_2SO_4 in 500 mL of Milli-Q Water)
Mobile phase Ratio	100 % v/v
Flow rate	0.3 mL/min
Diluent	Milli-Q Water
Injection volume	20 µL
Column oven temperature	35 ºC
Auto sampler temperature	15 ºC
Detector	Photo Diode Array (PDA)
Lamp	D_2
Detection wavelength	210 nm
Software	LabSolutions
Run time	20 minutes
These were optimized chromatographic conditions which gives satisfactory results and lie well within acceptance criteria.	

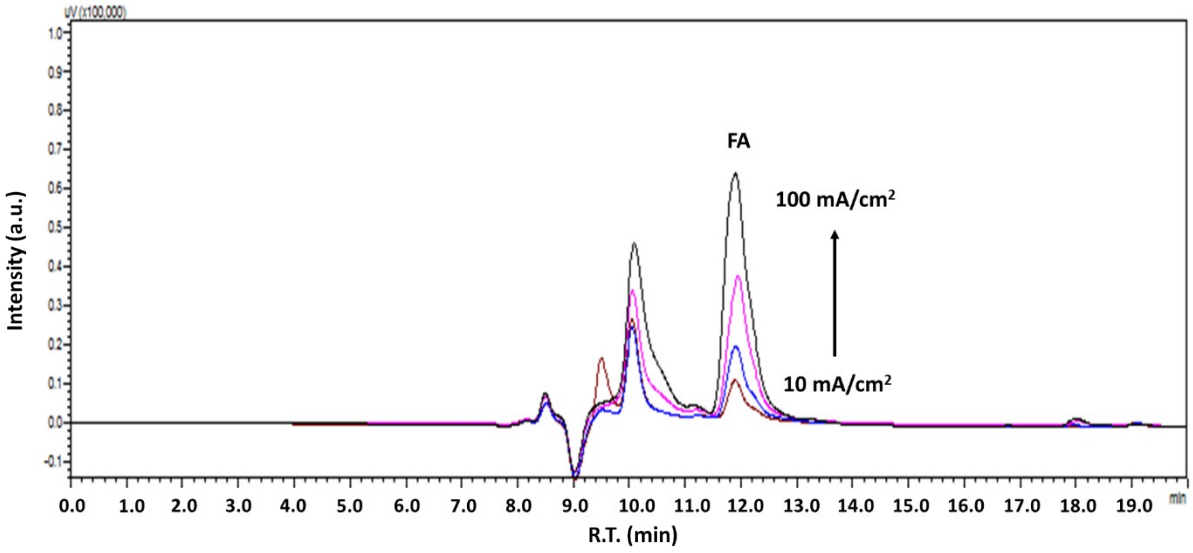

Figure S14-a Stack Chromatogram for conversion from EG to formate (FA) electrolyte at different current for 2 hours.

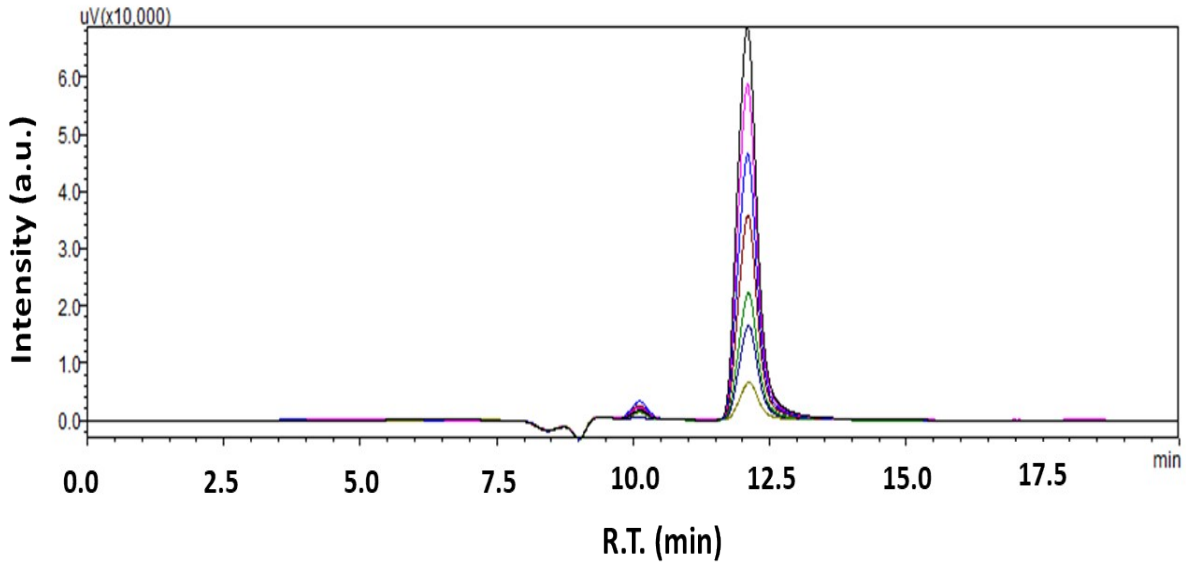

Figure S14-b Stack Chromatogram for formic acid standard for calibration curve for quantification.

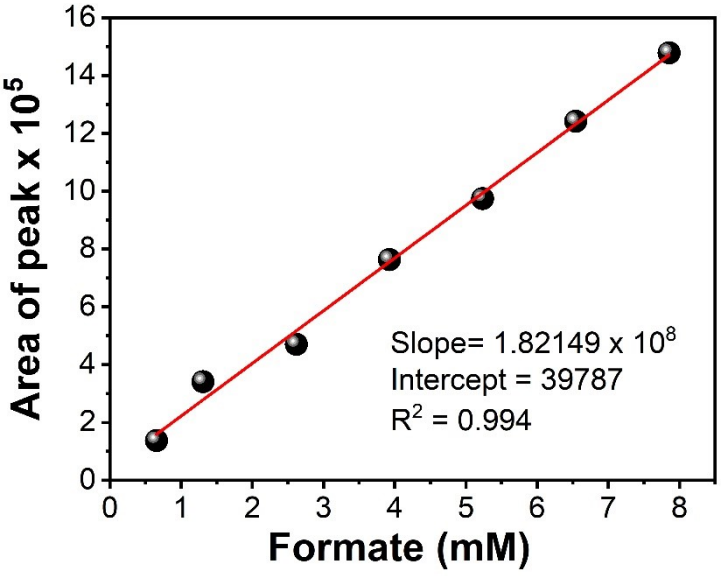

Figure S14-c Calibration curve for quantification of the formate.

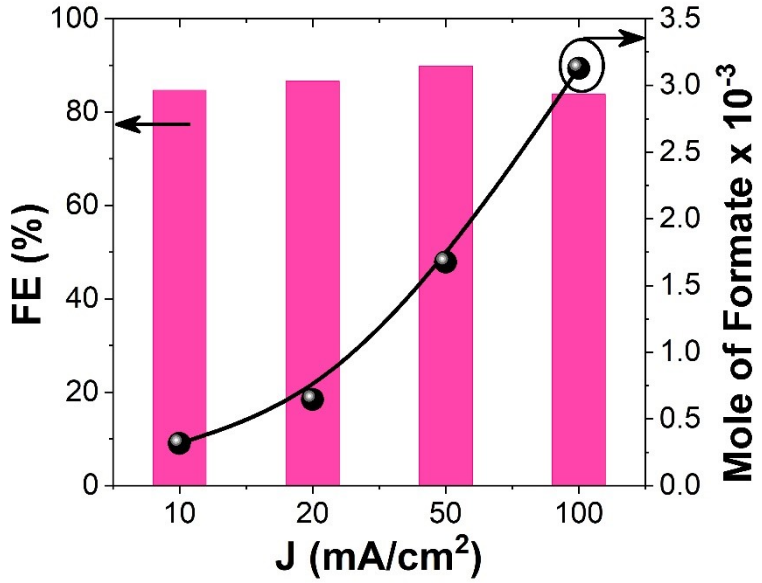

Figure S14-d Mole of formate produced by anodic oxidation and faradic efficiency (FE) at different current densities (time of electrolysis = 2 hr).

Faradic Efficiency for the electrochemical conversion from ethylene glycol to formate was evaluated using following formula:

$$FE(\%) = \frac{2 \times mole\ of\ HCOOH \times 96485}{C} \times 100\%$$

Where, C = charge (C)

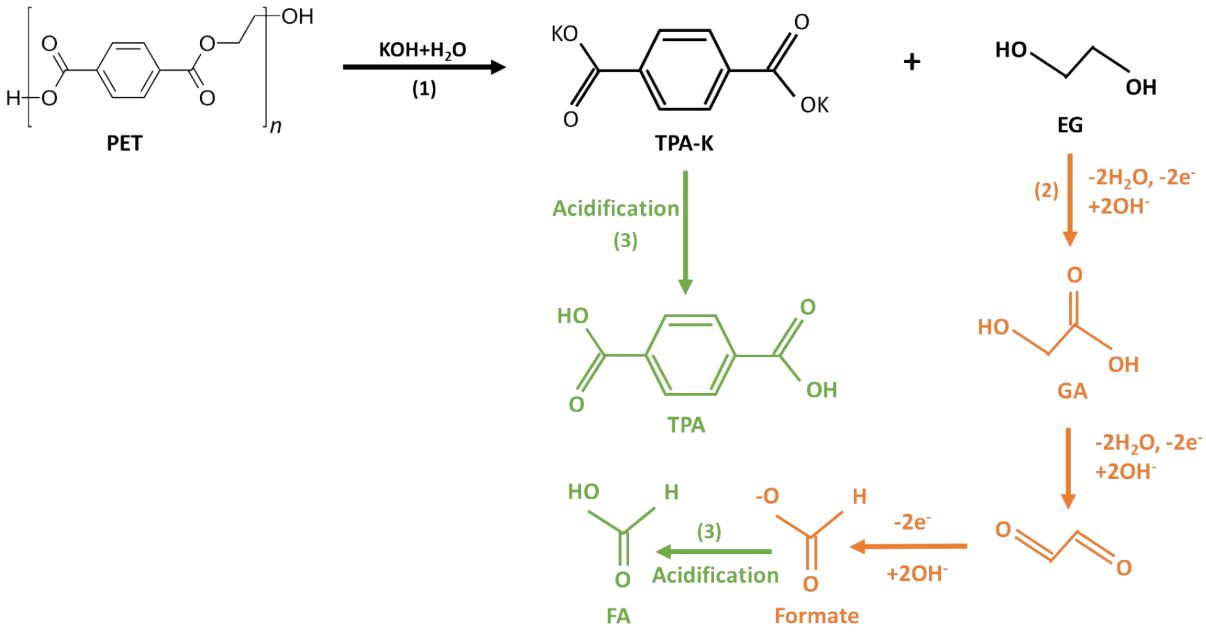

Figure S15 PET bottle upcycling process.

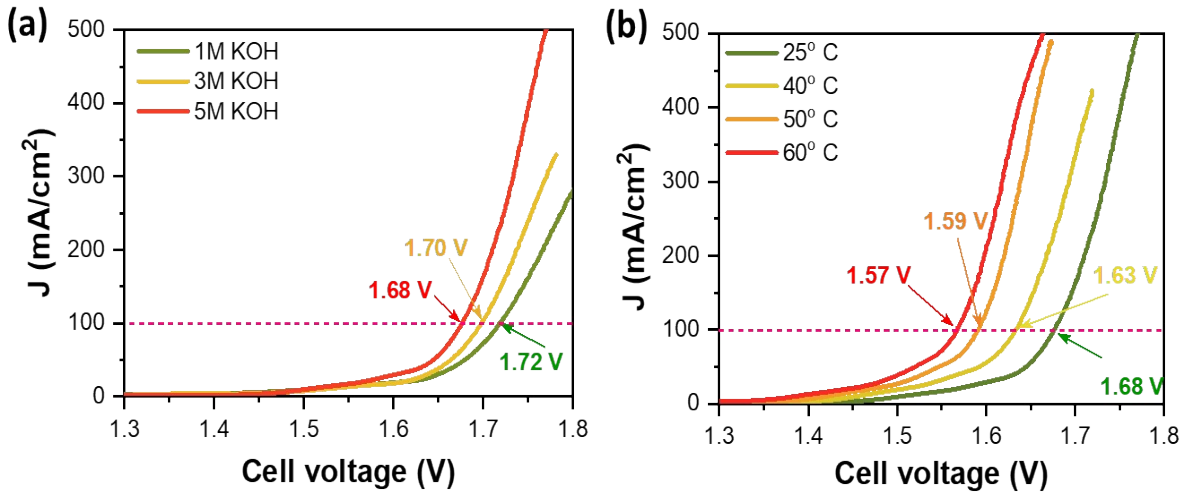

Figure S16 (a) Polarization curves for bi-functional water electrolysis on Ni-Fe_3Se_4 electrodes in 1M, 3M and 5M KOH at room temperature, and (b) Polarization curves for bi-functional water electrolysis on Ni-Fe_3Se_4 electrodes in 5M KOH at elevated temperatures.

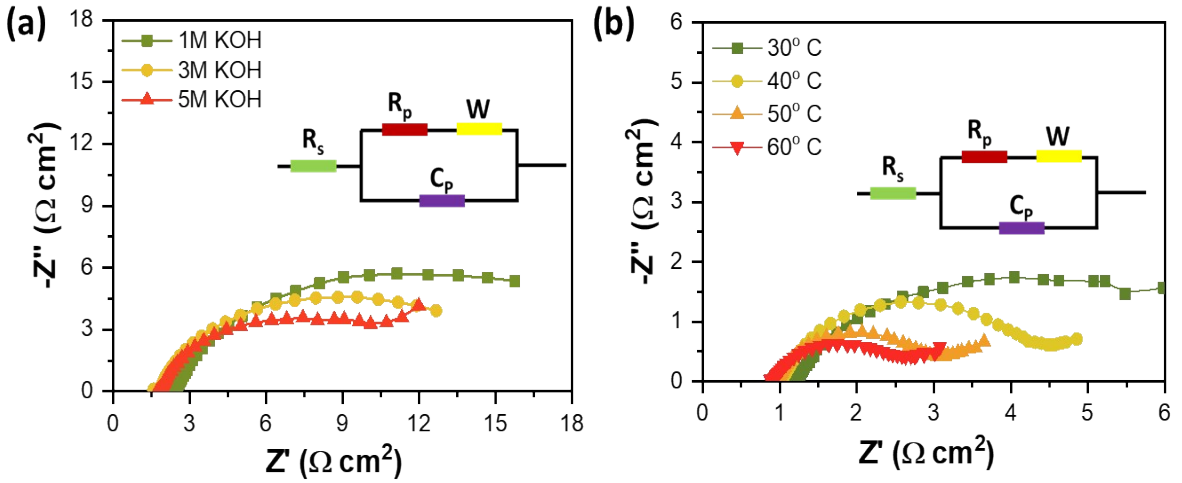

Figure S17 Nyquist plots for bi-functional water electrolysis recorded at cell voltage 1.5 V.

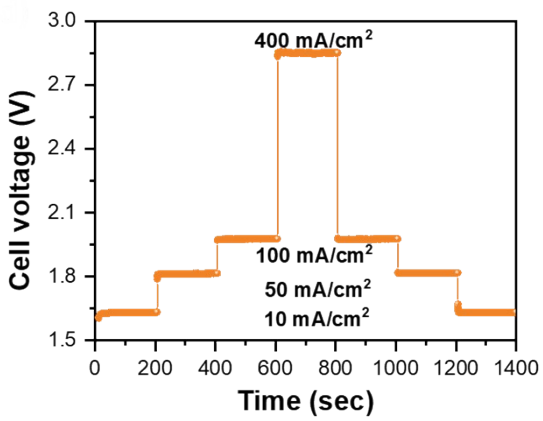

Figure S18 Multi-step chrono-potentiometry curve for bi-functional water electrolysis on Ni-Fe_3Se_4 electrode in 1M KOH at room temperature.

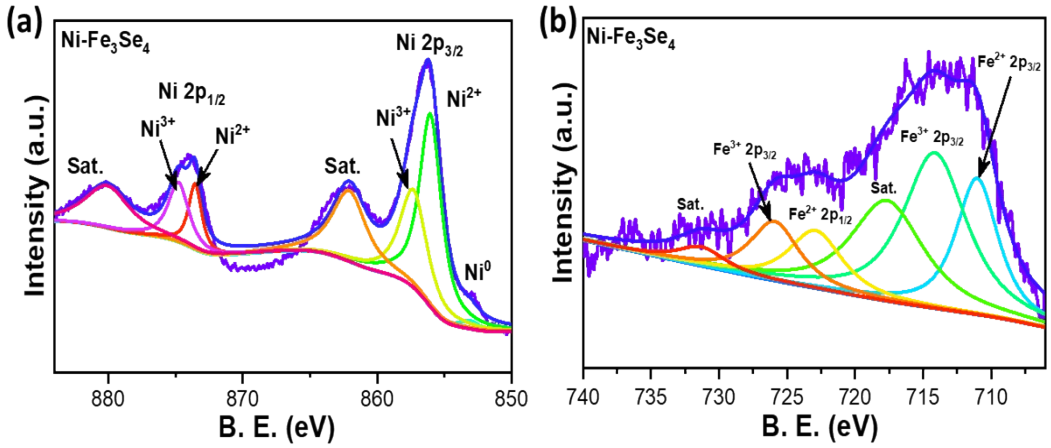

Figure S19 XPS spectra of Ni-Fe_3Se_4 after stability test.

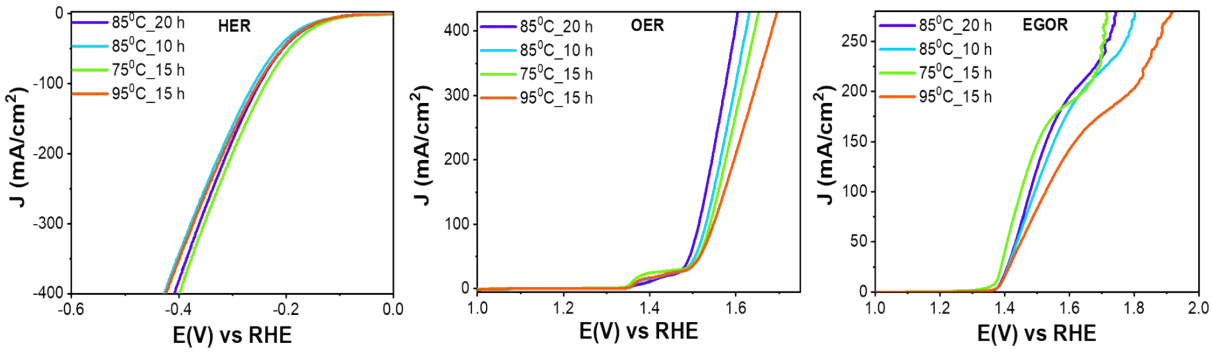

Figure S20 Polarization curves for HER, OER and EGOR performance of Ni-Fe_3Se_4 catalysts prepared with different synthesis time duration and temperature.

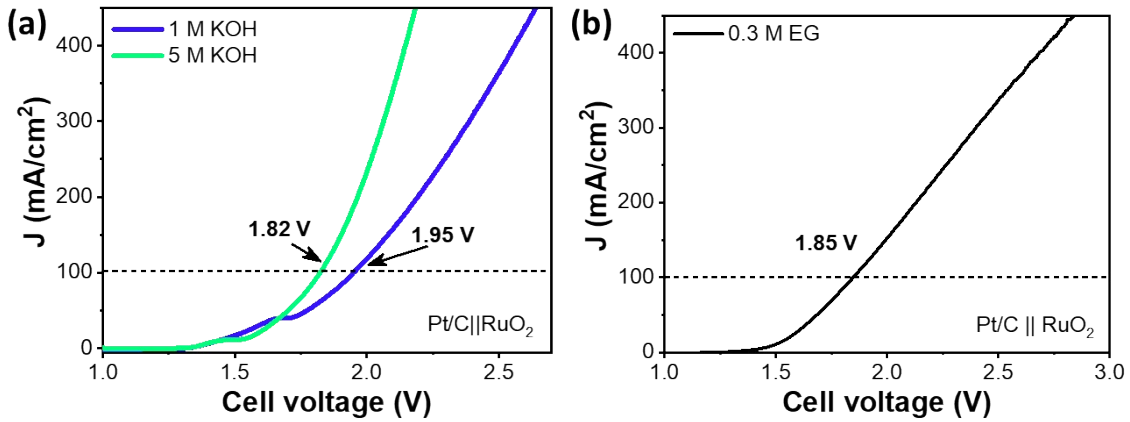

Figure S21 (a) Polarization curves for water electrolysis in 1M KOH and 5M KOH (b) Polarization curve in 1M KOH + 0.3 M EG of commercial Pt/C-RuO2 electrolyser

Table S1 Comparison of OER performance Fe_3Se_4 with previous reports on transition metal chalcogenides.

Catalysts	Overpotential (mV)	Tafel slope (mV/dec)	Ref.
Ni-Fe_3Se_4	164@10 mA/cm^2 222 @ 100 mA/cm^2	50.9	This work
CoFe-MOF-Se	270 @ 10 mA/cm^2	53.3	[12]
NiFeS	290@ 100 mA/cm^2	39	[3]
$ZnCo_2O_4$@NiFe LDH	249@10 mA/cm^2	96.7	[4]
Fe-CoNi LDHs	260@10 mA/cm^2	49	[11]
CoP@FeCoP	238@10 mA/cm^2	47.98	[5]
ZIF-12/Fe-Cu LDH	337@10 mA/cm^2	89	[10]
Ni_3Se_2@NF	315 @ 100 mA/cm^2	-	[1]
NiFeSe@NiSe/O@Carbon cloth	330 @ 10 mA/cm^2	63.2	[2]
(CoNi)Se_2@NiFe LDH nanocage	277 @ 10 mA/cm^2	75	[13]
NiFe/C	320@ 10 mA/cm^2	27	[6]
Ni-Fe LDH/CNT	234@ 10 mA/cm^2	30.7	[9]
Ni0.69Fe0.31Ox/C	280@ 10 mA/cm^2	30	[8]
Ni0.9Fe0.1O thin films	340@ 10 mA/cm^2	30	[7]

Table S2 Comparison of water electrolysis performance of $Ni_xFe_{3-x}Se_4$ with previous reports on transition metal chalcogenides.

Catalysts	Potential (V)@current density (mA/cm^2)	Ref.
Ni-Fe_3Se_4	1.72@100 in 1M KOH	This work
CoMoO//CoMoP NSs@NF	~ 1.9V@100 mA/cm^2	[14]
CoNi/$CoFe_2O_4$/NF	1.75V @ 100 mA cm^{-2}	[15]
$Co_{0.26}$-$Ni(OH)_2$/CF	1.73V@10 mA/cm^2 1.9V@100 mA/cm^2	[16]
NiCoFeB nanochains	1.81V@10 mA/cm^2 1.96V@100 mA/cm^2	[17]
B, N: Mo_2C@BCN	1.84V@100 mA/cm^2	[18]
CoMn/$CoMn_2O_4$	1.64V@10 mA/cm^2 1.91V@100 mA/cm^2	[19]

Table S3 Comparison of PET/EG electrolysis performance of $Ni_xFe_{3-x}Se_4$ with previous reports on transition metal chalcogenides.

Catalysts	PET treatment and Measurement condition	Potential (V)@current density (mA/cm^2)	Anode FE (%) (Formate)	Ref.
Ni-Fe_3Se_4	4 g PET Bottle + 50 ml 2M KOH 150°C for 15 hr [single cell]	1.49 V @ 10 mA/cm^2 1.60 V @ 50 mA/cm^2	89% @50 mA/cm^2	This work
OMS-Ni_1-CoP	6.3 g PET + 100 ml 2M KOH [Single cell]	1.52 V @ 10 mA/cm^2	96%	[20]
$CuCo_2O_4$/NF	5g PET + 50 ml 5M KOH [Membrane electrode assembly (MEA) flow cell]	1.56 V @ 100 mA/cm^2	93%	[21]
Ni_3N/W_5N_4	2.0 g PET bottle + 100 ml 4M KOH [AEM H-type cell]	1.47 V @ 50 mA/cm^2	85%	[22]
$NiCo_2O_4$/CFP	0.768 g PET powder was added in 40 mL of 1 M NaOH solution and autoclaved at 180°C for 2 h. [H-type cell (anion exchange membrane, AEM)]	1.9 V @ 20 mA/cm^2 Cathode:CO2RR	90%	[23]
CuO nanowire	0.77 g PET powder was added in 40 mL of 1 M KOH solution and autoclaved at 180°C for 2h	- [H-type cell]	88%	[24]

Table S4 Optimization of parameters for PET hydrolysis.

1.	4 g PET (waste bottle)	2M KOH (50 ml water)	160° C	15 h (~100% degradation)
2.	4 g PET (waste bottle)	2M KOH (50 ml water)	160° C	6 h (~20% degradation)
3.	4 g PET (waste bottle)	2M KOH (50 ml water)	160° C	10 h (~80% degradation)
4.	6 g PET (waste bottle)	2M KOH (60 ml water)	160° C	15 h (~100% degradation)
5.	4 g PET (waste bottle)	2M KOH (50 ml water)	120° C	15 h (~80% degradation)

Reference:

[1] A. Sivanantham, S. Shanmugam, Nickel selenide supported on nickel foam as an efficient and durable non-precious electrocatalyst for the alkaline water electrolysis,

Appl. Catal. B Environ. 203 (2017) 485–493. https://doi.org/https://doi.org/10.1016/j.apcatb.2016.10.050.

[2] G. Yilmaz, C.F. Tan, Y.-F. Lim, G.W. Ho, Pseudomorphic Transformation of Interpenetrated Prussian Blue Analogs into Defective Nickel Iron Selenides for Enhanced Electrochemical and Photo-Electrochemical Water Splitting, Adv. Energy Mater. 9 (2019) 1802983. https://doi.org/https://doi.org/10.1002/aenm.201802983.

[3] J. Wang, J.M. Barforoush, K.C. Leonard, Sulfur incorporation into NiFe oxygen evolution electrocatalysts for improved high current density operation, Mater. Adv. 4 (2023) 122–133. https://doi.org/10.1039/D2MA00902A.

[4] R. Que, S. Liu, Y. Yang, Y. Pan, High catalytic performance of core-shell structure ZnCo2O4@NiFe LDH for oxygen evolution reaction, Mater. Lett. 298 (2021) 129982. https://doi.org/https://doi.org/10.1016/j.matlet.2021.129982.

[5] J. Shi, F. Qiu, W. Yuan, M. Guo, Z.-H. Lu, Nitrogen-doped carbon-decorated yolk-shell CoP@FeCoP micro-polyhedra derived from MOF for efficient overall water splitting, Chem. Eng. J. 403 (2021) 126312. https://doi.org/https://doi.org/10.1016/j.cej.2020.126312.

[6] A. Sakamaki, M. Yoshida-Hirahara, H. Ogihara, H. Kurokawa, One-Step Synthesis of Highly Active NiFe Electrocatalysts for the Oxygen Evolution Reaction, Langmuir. 38 (2022) 5525–5531. https://doi.org/10.1021/acs.langmuir.2c00097.

[7] L. Trotochaud, J.K. Ranney, K.N. Williams, S.W. Boettcher, Solution-Cast Metal Oxide Thin Film Electrocatalysts for Oxygen Evolution, J. Am. Chem. Soc. 134 (2012) 17253–17261. https://doi.org/10.1021/ja307507a.

[8] Y. Qiu, L. Xin, W. Li, Electrocatalytic Oxygen Evolution over Supported Small Amorphous Ni–Fe Nanoparticles in Alkaline Electrolyte, Langmuir. 30 (2014) 7893–7901. https://doi.org/10.1021/la501246e.

[9] M. Duan, M. Qiu, S. Sun, X. Guo, Y. Liu, X. Zheng, F. Cao, Q. Kong, J. Zhang, Intercalating assembly of NiFe LDH nanosheets/CNTs composite as high-performance electrocatalyst for oxygen evolution reaction, Appl. Clay Sci. 216 (2022) 106360. https://doi.org/https://doi.org/10.1016/j.clay.2021.106360.

[10] A. Hameed, M. Batool, W. Iqbal, S. Abbas, M. Imran, I.A. Khan, M.A. Nadeem, ZIF-12/Fe-Cu LDH Composite as a High Performance Electrocatalyst for Water Oxidation, Front. Chem. 9 (2021). https://doi.org/10.3389/fchem.2021.686968.

[11] Y. Shi, J. Li, B. Zhang, S. Lv, T. Wang, X. Liu, Tuning electronic structure of CoNi LDHs via surface Fe doping for achieving effective oxygen evolution reaction, Appl. Surf. Sci. 565 (2021). https://doi.org/10.1016/j.apsusc.2021.150506.

[12] Z. Shang, T. Li, B. Hu, M. Liu, W. Lu, F. Yu, Y. Zheng, Two-dimensional bimetallic selenium-containing metal-organic frameworks and their calcinated derivatives as electrocatalysts for overall water splitting, Front. Energy. (2024). https://doi.org/10.1007/s11708-024-0924-x.

[13] J.-G. Li, H. Sun, L. Lv, Z. Li, X. Ao, C. Xu, Y. Li, C. Wang, Metal–Organic Framework-Derived Hierarchical (Co,Ni)Se2@NiFe LDH Hollow Nanocages for Enhanced Oxygen Evolution, ACS Appl. Mater. Interfaces. 11 (2019) 8106–8114. https://doi.org/10.1021/acsami.8b22133.

[14] Y. Zhang, Q. Shao, S. Long, X. Huang, Cobalt-molybdenum nanosheet arrays as highly efficient and stable earth-abundant electrocatalysts for overall water splitting, Nano Energy. 45 (2018) 448–455.

[15] S. Li, S. Sirisomboonchai, A. Yoshida, X. An, X. Hao, A. Abudula, G. Guan, Bifunctional CoNi/CoFe 2 O 4/Ni foam electrodes for efficient overall water splitting at a high current density, J. Mater. Chem. A. 6 (2018) 19221–19230.

[16] C.B. Sun, M.W. Guo, S.S. Siwal, Q.B. Zhang, Efficient hydrogen production via urea electrolysis with cobalt doped nickel hydroxide-riched hybrid films: Cobalt doping effect and mechanism aspect, J. Catal. 381 (2020) 454–461. https://doi.org/https://doi.org/10.1016/j.jcat.2019.11.034.

[17] Y. Li, B. Huang, Y. Sun, M. Luo, Y. Yang, Y. Qin, L. Wang, C. Li, F. Lv, W. Zhang, Multimetal borides nanochains as efficient electrocatalysts for overall water splitting, Small. 15 (2019) 1804212.

[18] M.A.R. Anjum, M.H. Lee, J.S. Lee, Boron-and nitrogen-codoped molybdenum carbide nanoparticles imbedded in a BCN network as a bifunctional electrocatalyst for hydrogen and oxygen evolution reactions, ACS Catal. 8 (2018) 8296–8305.

[19] D. Zheng, Z. Jing, Q. Zhao, Y. Kim, P. Li, H. Xu, Z. Li, J. Lin, Efficient Co-doped pyrrhotite Fe0. 95S1. 05 nanoplates for electrochemical water splitting, Chem. Eng. J. 402 (2020) 125069.

[20] N. Wang, X. Li, M.-K. Hu, W. Wei, S.-H. Zhou, X.-T. Wu, Q.-L. Zhu, Ordered macroporous superstructure of bifunctional cobalt phosphide with heteroatomic modification for paired hydrogen production and polyethylene terephthalate plastic recycling, Appl. Catal. B Environ. 316 (2022) 121667. https://doi.org/https://doi.org/10.1016/j.apcatb.2022.121667.

[21] F. Liu, X. Gao, R. Shi, E.C.M. Tse, Y. Chen, A general electrochemical strategy for upcycling polyester plastics into added-value chemicals by a CuCo2O4 catalyst, Green Chem. 24 (2022) 6571–6577. https://doi.org/10.1039/D2GC02049A.

[22] F. Ma, S. Wang, X. Gong, X. Liu, Z. Wang, P. Wang, Y. Liu, H. Cheng, Y. Dai, Z. Zheng, B. Huang, Highly efficient electrocatalytic hydrogen evolution coupled with upcycling of microplastics in seawater enabled via Ni3N/W5N4 janus nanostructures, Appl. Catal. B Environ. Energy. 307 (2022) 121198. https://doi.org/https://doi.org/10.1016/j.apcatb.2022.121198.

[23] J. Wang, X. Li, M. Wang, T. Zhang, X. Chai, J. Lu, T. Wang, Y. Zhao, D. Ma, Electrocatalytic Valorization of Poly(ethylene terephthalate) Plastic and CO2 for Simultaneous Production of Formic Acid, ACS Catal. 12 (2022) 6722–6728. https://doi.org/10.1021/acscatal.2c01128.

[24] J. Wang, X. Li, T. Zhang, Y. Chen, T. Wang, Y. Zhao, Electro-reforming polyethylene terephthalate plastic to co-produce valued chemicals and green hydrogen, J. Phys. Chem. Lett. 13 (2022) 622–627.